Published with doi: 10.1061/(ASCE)BE.1943-5592.0001311

Girder-Deck Interface: Partial Debonding, Deck Replacement, and Composite Action

Chaohui Li, Ph.D., IDC Consulting Engineers, Inc.
Rémy D. Lequesne, Ph.D., P.E., University of Kansas
Adolfo Matamoros, Ph.D., P.E., University of Texas at San Antonio

ABSTRACT

Results are reported from tests of three precast/prestressed concrete girders under fatigue-type cyclic and monotonic loading conducted after deck removal and replacement. Although deck demolition altered the top surface of the girders, the girder-deck interfaces exhibited shear strengths greater than their nominal capacity (based on the 2012 AASHTO LRFD Specification) after 2×10^6 cycles of loading to 45 and 30% of their nominal strength for troweled and roughened interfaces, respectively. A partially debonded detail was used for two of the girders to protect the girder top flange, which was wide and thin, during deck demolition. The roofing felt used to debond the girder-deck interface over the flanges reduced the effort required for deck removal by 65% compared with the typical detail, eliminated chipping-hammer induced damage to the girder flanges, and still resulted in sustained composite action under 2×10^6 cycles of loading. The width of bonded interface had little effect on girder stiffness and no observed effect on the width of deck effective in bending.

INTRODUCTION

Composite action between bridge girders and a bridge deck depends on resistance to shearing along the horizontal girder-deck interface. This resistance is a result of bonding and mechanical interlock at the joint and transverse reinforcement perpendicular to the girder axis. Composite action increases the stiffness and strength of the system, but the bonding of concrete at the cold joint also makes deck removal and replacement more difficult. This is especially true for girders with wide and thin top flanges (Fig. 1), which are prone to damage during deck removal. Furthermore, it is not clear how deck removal and replacement affects the behavior of girders under fatigue-type cyclic and monotonic loadings.

The hypothesis evaluated in this study is that partially debonding the girder-deck interface can simplify deck removal and protect the vulnerable tips of wide and thin girder flanges without compromising composite action. This was evaluated through tests of NU I-Girders with 75 mm [3 in.] thick and 1220 mm [48 in.] wide top flanges under repeated and monotonic loadings. Three girders were tested, each with one of the following top flange surface finishes: fully troweled, fully troweled except for 200 mm [8 in.] of roughened concrete (to an amplitude of 6 mm [0.25 in.]) over the girder web, and roughened over the entire surface except for 150 mm [6 in.] of troweled concrete at the flange tips, which represents common practice (resulting in a 910 mm [36 in.] width of roughened concrete). The girders were subjected to three phases of testing: 1) deck removal and replacement to study constructability, 2) fatigue testing under 2 million cycles of repeated load, and 3) monotonic loading to failure.

Composite Action

Precast bridge girders are designed to act compositely with the bridge deck to increase the stiffness and strength of the system and thereby allow for reduced girder depths. This composite action relies on resistance to shearing along the girder-deck interface, which is a function of interface roughness and transverse reinforcement amount (Hanson 1960; Saemann and Washa 1964) as well as concrete compressive strength (Loov and Patnaik 1994; Kahn and Slapkus 2004). Tests of girders monotonically loaded to failure have shown that slip and transverse reinforcement stresses are negligible until cracks develop along the interface. After cracking, tests by Hanson (1960) showed that composite action was maintained until an interfacial slip of approximately 0.13 mm [0.005 in.] developed, beyond which shear strength quickly deteriorated.

Tests of composite girders under repeated loading have been conducted to study the fatigue resistance of the girder-deck connection under up to two million cycles of simulated traffic loads. As with monotonically loaded beams, these tests have shown that fatigue performance is improved by roughening the top flange of the girder (to an amplitude of at least 6 mm [0.25 in.]) and increasing the amount of transverse reinforcement (Badoux and Hulsbos 1967). Chung and Chung (1976) showed that composite action in girders with rough bonded interfaces degraded under repeated loading when loads exceeded 55 percent of the pseudo-static strength. Their results also showed that composite action deteriorated quickly after an interfacial slip of 0.025 mm [0.001 in.] developed, a much smaller value than observed by Hanson in tests of monotonically loaded beams.

Based on these and other studies, composite action is relatively well understood and design methods for achieving composite action are well established and codified in the AASHTO LRFD Specification (2012) and ACI Building Code (2014). Nevertheless, the performance of composite beams with partially debonded interfaces is not well understood because few tests have been conducted on such specimens. The only researchers found to have conducted such tests were

Chung and Chung (1976), who used aluminum strips painted with grease to reduce the girder-deck contact area to ensure specimen interface failure during tests. Additional tests are therefore necessary before specifications for a partially debonded detail can be adopted in practice. Furthermore, the authors are not aware of any studies investigating the fatigue performance of composite girders after bridge decks have been removed and replaced. Given the widespread need to extend the service-life of existing infrastructure, data are needed to better understand the long-term performance of repaired bridges.

Deck Removal

Procedures for bridge deck removal differ depending on whether the portion of deck being removed is located between girders or over a girder. Removal of the deck between girders is mainly done by saw cutting longitudinally (parallel to the girders) through the thickness of the deck alongside the tips of the girder flanges and then lifting the saw-cut concrete to the ground (Assad and Morcous 2015). This process is relatively fast and does not damage girders.

Removal of deck concrete over girders is more time-consuming due to the strength of the connection between the deck and girder and the goal of protecting the girders for continued use. Typical methods, like hydro-demolition and use of jackhammers and other chipping equipment, are not well suited for use over wide and thin girder flanges (characteristic of NU I-Girders, which have 75 mm [3 in.] thick flanges). Furthermore, not only are the thin flanges vulnerable to impact damage, but the contact area between the NU I-Girders and a deck is significantly larger than for other girder types, increasing the effort required for demolition. To protect girders, the type and size of chipping equipment is often limited to no greater than 130 N [30 lbs] when used over precast girders. In Kansas, hammers are limited to 67 N [15 lbs] for removing concrete near the top girder flange (KDOT 2015).

Large reductions in top flange area can negatively affect the structural performance of the composite system after the deck is replaced, particularly if the composite girder is slender (Assad and Morcous 2015). To reduce the risk of top flange damage, a connection detail was proposed for girders with wide and thin top flanges (Kamel 1996) wherein the entire top flange is debonded using a spray-on debonding agent and shear strength is provided by a series of shear keys (indentations transverse to the girder axis) and transverse reinforcement. Although effective, the detail has not been frequently used in practice because of concerns about making the thin flange even thinner with deep indentations. There is therefore need for a simple connection detail that facilitates concrete deck removal while ensuring composite action.

EXPERIMENTAL PROGRAM

Three precast prestressed girder specimens were delivered to the laboratory, where reinforced concrete bridge decks were cast onto the top flanges. The girders were then subjected to three phases of testing: 1) deck removal and replacement, 2) fatigue testing under 2 million cycles of repeated load, and 3) monotonic loading to failure. Specimen details are described below, followed by detailed descriptions of each testing phase.

Specimen Details

Three NU900 [U.S. NU35] girders (Fig. 2) were fabricated by a local precast concrete supplier and delivered to the laboratory. NU900 girders are the shallowest of the NU series of I-Girders that have been used since the 1990s in several U.S. states and Canadian provinces due to their structural efficiency, economy, and aesthetic appeal (Beacham and Derrick 1999). The top flange of each girder was finished in accordance with one of the three details shown in Fig. 3: Girder #1 had a fully troweled surface, Girder #2 was troweled except for a 200 mm [8 in.] wide strip over the web that was roughened, and Girder #3, which represents current practice, had a fully roughened surface except for 150 mm [6 in.] wide strips along the edges of both flange tips. The roughened portions of Girders #2 and #3 were roughened to an amplitude of approximately 6 mm [0.25 in.] using a rake at the precast plant. Reinforcement consisting of 16 mm [No. 5] hooked bars spaced at 300 mm [12 in.] crossed the girder-deck interface in all specimens. These details were selected to examine the effect of three different surface preparations on constructability and composite girder behavior. The nominal shear strengths of these connections, divided by the area of concrete engaged in shear transfer, were 2.1, 4.6, and 2.6 MPa [300, 660, and 370 psi] for Girders #1, #2, and #3, based on Eq. 1, as found in Section 5.8.4.1 of the AASHTO Specification (2012) (see Notation section). This resulted in calculated forces on the girders at failure of 580, 1250, and 3070 kN [130, 280, and 690 kips].

$$V_{ni} = cA_{cv} + \mu_{AASHTO}\left(A_{vf}f_y + P_c\right) \leq \min[K_1 f_c' A_{cv}, K_2 A_{cv}] \qquad \text{Eq. 1}$$

For roughened surfaces (Girders #2 and #3), c is 1.9 MPa [0.28 ksi], μ_{AASHTO} is 1.0, K_1 is 0.3, and K_2 is 12 MPa [1.8 ksi] according to the AASHTO Specification (2012). For smooth surfaces (Girder #1), c is 0.5 MPa [0.075 ksi], μ_{AASHTO} is 0.6, K_1 is 0.2, and K_2 is 5.5 MPa [0.8 ksi]. The widths of the engaged concrete surfaces were 200 mm [8 in.] for Girders #1 and #2 and 910 mm [36 in.] for Girder #3; P_c was zero.

Elevation and cross-sectional views of the NU900 girders are shown in Fig. 1. Girders #1 and #2 were designed so that the flexural and transverse (web) shear strengths of the composite girder, calculated in accordance with the AASHTO Specification (2012), exceeded the demand associated with the interface shear strength of the girder-deck connection for a simply supported girder loaded at midspan (Fig. 2). Girder #3 was instead designed to fail in flexure because it was not possible to achieve failure at the girder-deck interface without exceeding the maximum permitted web shear stress. Each specimen had 18 straight 15 mm [0.6 in.] diameter seven-wire low-relaxation strands, with 16 strands distributed within the bottom flange and two strands placed 130 mm [5 in.] below the top of the precast girder (Fig. 1). The nominal flexural strength of the girders was 680 kN-m [500 kip-ft], which would be reached at an applied load of 2360 kN [530 kips]. The strands placed near the top of the section were included to ensure that the tensile stress in the top flange at tendon release remained below an allowable stress of 1.7 MPa [240 psi]. This limit corresponded to the allowable stress permitted in the AASHTO Specification (2012) (and ACI Building Code (2014)) of $0.25\sqrt{f'_{ci}}$, MPa [$0.0948\sqrt{f'_{ci}}$, ksi]. Mild steel welded wire fabric (WWR5) was also provided in the top flanges of the girders.

Design for web shear was done using the provisions for simplified shear design in the AASHTO Specification (2012). Transverse reinforcement consisted of 16 mm [No. 5] bars spaced at 300 mm [12 in.] for Girders #1 and #2, and at 150 mm [6 in.] for Girder #3. The nominal shear strength of Girders #1 and #2 was 760 kN [170 kips], which would be reached at an applied force of 1500 kN [340 kips]. The nominal shear strength of Girder #3 was 1070 kN [240 kips], which would be reached at an applied force of 2140 [480 kips]. The end zones of the specimens, beyond the location of the supports, had 16 mm [No. 5] transverse reinforcing bars spaced at 50 mm [2 in.] to prevent bond-related failures.

After girder delivery, reinforced concrete bridge decks were constructed on each specimen in the laboratory. As shown in Fig. 2, the precast girders were 8.2 m [27 ft] long and 900 mm [35.4

in.] deep. The decks were 4.3 m [170 in.] long and 180 mm [7 in.] thick. The deck was cast shorter than the beam span so the connection between deck and girder would limit the strength of some of the specimens, allowing study of the connection. The deck was reinforced with two mats of 16 mm [No. 5] bars. Bars in the top mat were spaced at 530 and 610 mm [21 and 24 in.] perpendicular and parallel to the girder axis, respectively, greater than the maximum permitted spacing of 460 mm [18 in.] so that the target reinforcement ratio could be maintained. Exceeding the maximum spacing is not expected to have affected study outcomes. The bottom bars were spaced at 360 and 410 mm [14 and 16 in.] perpendicular and parallel to the girder axis, respectively. This reinforcement was close to the minimum of 380 and 570 mm^2/m [0.18 and 0.27 $in.^2/ft$] for top and bottom reinforcement, respectively, required in Section 9.7.2.5 of the AASHTO Specification (2012). The topmost and bottommost layers of deck reinforcement were oriented perpendicular to the girder axis (in the direction of deck spans).

Material Properties

Concrete mixture proportions used for the girders and bridge decks are shown in Table 1. The girder and deck concretes had specified compressive strengths of 55 and 28 MPa [8 and 4 ksi], respectively. Concrete compressive strength for the girder concrete, reported by the manufacturer, was 49.6 MPa [7.2 ksi] at tendon release (19 hours after placement) and 65.5 MPa [9.5 ksi] on the day the girders were shipped (8 days). Deck concrete had average measured compressive strength of 33.8 MPa [4.9 ksi] at the time of demolition (34 days after placement) and 35.2 MPa [5.1 ksi] at the time of the monotonic tests (417 days after placement). Compressive strength was taken as the average strength of three 100 by 200 mm [4 by 8 in.] cylinders tested in accordance with the provisions of ASTM C39.

The NU900 [NU35] girders were constructed with Grade 420 [Grade 60] mild steel reinforcement compliant with ASTM A615 and Grade 1860 [Grade 270] 15 mm [0.6 in.] diameter seven-wire low-relaxation strands compliant with ASTM A416. Web reinforcement and interface shear reinforcement were epoxy coated. Reinforcement used to fabricate the deck was uncoated Grade 420 [Grade 60] mild steel reinforcement, compliant with ASTM A615, with a measured yield stress of 455 MPa [66 ksi].

Organic felt, referred to herein as roofing felt, was used to debond portions of the girder-deck interface. It was a 1 mm [0.04 in.] thick asphalt-saturated organic felt that conformed to ASTM D4869.

Phase 1: Bridge Deck Casting, Removal, and Replacement

Deck Casting

A 180 mm [7 in.] thick slab was cast onto each of the girders to simulate a bridge deck. The bridge deck had a width equal to the girder top flange and a length of 4.3 m [170 in.]. Prior to assembly of the deck reinforcement, roofing felt was placed over the troweled portions of the flange of Girder #2 (Fig. 4). No adhesive was used to hold the roofing felt in place, although a small amount may be necessary in the field. Although alternatives to roofing felt were considered, including spray-on debonding agents, feedback from contractors and collaborators at the Kansas Department of Transportation indicated that use of spray-on debonding agents might be problematic in practice.

For this first concrete placement, no roofing felt was used for Girders #1 or #3 so it would be possible to compare the effort required to remove deck concrete bonded to troweled and roughened concrete surfaces with the effort required to remove concrete cast over roofing felt.

Concrete from a local ready-mix supplier was delivered with a single mixer transport truck, placed into the formwork for all three decks using a bucket and crane, and mechanically consolidated. Concrete was cured using damp burlap and plastic sheets for three days. Formwork was removed between four and five days after casting.

Deck Demolition Process

Bridge decks were removed from the girders beginning approximately 28 days after placement. The level of effort required for bridge deck removal and the damage caused by it were documented. The primary tools used for deck removal were a walk-behind concrete saw, a 290 N [65 lb] electric jackhammer with a 29 mm [1-1/8 in.] bit, a demolition hammer with an adjustable impact energy output from 5 to 25 J [3.7 to 18.5 foot-pounds], and hammers and chisels. Although the decks were new, it is believed the conclusions are applicable to older and deteriorated decks. Complications related to deterioration are outside the scope of this study.

The first step was to cut the deck using the walk-behind saw. Two longitudinal cuts were made in each deck 100 mm [4 in.] from the centerline of the girder (near to but not interfering with the interface shear reinforcement) and three transverse cuts were made at regular intervals (spaced at 1080 mm [42.5 in.]). The depth of cut was set to 170 mm [6.75 in.] to avoid contacting the girder top flange. Photos of decks shown in Fig. 5 were taken after saw cutting.

Removal of the deck sections located above the girder web, linked to the girder by bond and reinforcement crossing the interface, required greater effort than removal of the deck sections located over the flanges (referred to as edge sections), which had no interface reinforcement. For demolishing the edge sections, hammers, chisels, pry bars, and demolition hammers were used to break the deck concrete free from the girder top flange and, where necessary, demolish the deck concrete. For Girder #2, which had roofing felt placed over a large portion of the flanges, all eight saw-cut edge sections of the deck were easily detached by hammering chisels into the gaps created by saw-cutting or by using a demolition hammer to widen the gap between the deck and girder to break the deck loose (Fig. 5(a)). After being detached, these deck sections could be lifted off the girder and disposed of. For Girder #1, which had a troweled flange and no roofing felt (for this part of the study), it was possible to detach six of the eight edge sections using these procedures. For the two remaining edge sections of Girder #1 that could not be detached, and for seven of the eight edge sections on Girder #3 with a roughened top flange at the cold joint, it was necessary to use the demolition hammer to break apart the deck directly, as shown in Fig. 5(b).

The middle portions of the deck located over the beam webs were removed after the edge sections. This was done by first using a 290 N [65 lb] jackhammer to break the concrete down to the level of the interface reinforcement. Although such large equipment is typically not permitted for this application, it may be acceptable under certain conditions (such as for portions of the deck located directly over the girder web and to a depth not greater than the top deck reinforcement. A variable impact demolition hammer set to an impact energy level consistent with a 67 N [15 lb] hammer was then used to remove the remaining concrete down to the top of the girder flange.

Demolition Effort, Girder Damage, and Resulting Surface Roughness

The effort required for bridge deck demolition was quantified in terms of the person-hours required to complete the task in the laboratory (Table 2). Although the reported person-hours are not meant to be representative of the productivity of contractors on-site, they allow for relative comparisons of effort between specimens. Bridge deck demolition was performed by the same two workers to reduce variability caused by differences in the pace of work. The reported person-hours are separated into three parts: saw cutting, demolishing/removal of edge sections (over the flanges), and demolishing/removal of the middle portions of the deck over the web. As shown in Table 2, the effort spent on saw cutting and demolishing the middle sections (4.5 and 9.5 hours, respectively) were nominally the same for the three connection details. However, significant differences were documented in the effort required to demolish the edge portions of the decks. The effort required for bridge deck removal in Girders #1 and #2 was approximately 75% and 35% of that required for Girder #3, respectively.

Although the girders were generally in good condition after bridge deck demolition, several examples of damage were observed. Damage to the girder top flange and interface shear reinforcement occurred in Girders #2 and #3, respectively, due to contact with the saw blade. Other types of damage, shown in Fig. 6, were caused by chipping hammer impacts. Figure 6(a) shows damage to Girder #1 where a portion of the top flange surface was dislodged along with the deck concrete. The result was an approximately 13 by 250 by 410 mm [0.5 by 10 by 16 in.] crater in the thin top flange. Although this type of damage is effectively repaired when the replacement bridge deck is cast over the existing girder surface, it is an indication of the difficulty with which bridge deck concrete is separated from a troweled girder flange. In Girder #3 a through-thickness wedge-shaped section of the flange tip (approximately 190 by 64 mm [7.5 by 2.5 in.]) was dislodged due to accidental contact between the chipping hammer and the thin top flange (Fig. 6(b)), illustrating the vulnerability of the thin flanges to impact damage. Welded wire flange reinforcement was exposed, which would have to be repaired in the field to protect the exposed reinforcement.

The condition of the top surface of the girders was different after deck removal than prior to deck casting. Despite the changes, it was the judgement of the research team that classification of the flange top surface roughness (as troweled, roughened, etc.) was not changed by the process of casting and removal of the bridge deck. Although the surface roughness of the girders after finishing at the plant (6 mm [0.25 in.] amplitude using a rake) was not visible after deck removal, a roughened surface with an amplitude of approximately 6 mm [0.25 in.] was present due to peaks and valleys caused by the demolition hammer and small remnants of deck concrete. With some care, it is possible to create a post-deck-removal surface condition that would qualify as roughened according to AASHTO Specification (2012) requirements (a clean concrete surface, free of laitance, with surface roughened to an amplitude of 6 mm [0.25 in.]). Surfaces that were initially troweled were mostly smooth (similar to a troweled surface) after deck removal, but there were small peaks and divots where small pieces of deck concrete remained or where the deck removal process had removed some girder concrete. Parts of the troweled surfaces achieved sufficiently high bond with the deck to make damage to the girder unavoidable during deck demolition. Where roofing felt had been placed, the girder surface after demolition was unaffected by deck casting and removal, except for one minor instance of saw-cut damage to the girder flange. The roofing felt therefore effectively protected the girder from the casting process and deck removal.

Deck Recasting

Three weeks after bridge deck removal, replacement bridge decks were cast onto each girder. The dimensions, reinforcement, and concrete mixture proportions were the same used in the original decks. Figure 7 shows the surface preparation and deck reinforcement arrangement before casting the replacement decks. Girder surface preparation was the same used in the initial deck placement for Girders #2 and #3, but different for Girder #1, where roofing felt was applied on the edges of the flanges leaving a 200 mm [8 in.] wide troweled surface exposed over the web. This change was made so that a direct comparison between Girders #1 and #2 would provide a measure of the effect of roughening the strip of concrete over the girder web.

Phase 2: Fatigue Testing

Test Setup, Instrumentation, and Loading Protocol

Each of the three girders was subjected to 2 million cycles of simulated traffic load. The test setup and instrumentation used for these tests are shown in Fig. 2. The composite girder specimens were simply supported. A hydraulic actuator with a capacity of 490 kN [110 kips] was used to apply a cyclic force to the top of the beam at midspan, directly over the beam web. A 25 mm [1 in.] thick steel plate was placed between the actuator head and concrete deck. A bed of gypsum cement was placed between steel plates and concrete surfaces.

The girder was instrumented with three 13-mm-[0.5-in.]-stroke linear variable differential transformers (LVDTs) and 14 foil-type strain gauges fixed to the surface of the concrete. One LVDT was placed under the center axis of the girder at midspan to measure deflection. An LVDT was also placed at each end of the deck to measure relative slip between the deck and girder. The strain gauges used for this study were 120-ohm electrical resistance foil-type gauges with a gauge length of 20 mm [0.79 in.]. Six strain gauges were placed along the vertical axis at midspan at depths of 0, 13, 150, 200, 530, and 1020 mm [0, 0.5, 6, 8, 21, and 40 in.] from the top of the deck concrete. The strain gauge placed on the top surface of the deck at midspan was 380 mm [15 in.] away from the center axis of the beam, or 230 mm [9 in.] inboard from the side of the deck. Eight strain gauges were placed away from midspan in pairs along the deck-girder interface. Each pair included one gauge located above the interface and one below the interface. Each of the eight strain gauges was located 25 mm [1 in.] from the interface. Infrared markers shown in Fig. 2 were added prior to the final monotonic loading of the specimen to failure (described later), but were not used for the fatigue tests.

The loading protocol consisted of 2×10^6 cycles of sinusoidal force ranging between 36 and 360 kN [8 and 80 kips], for a load range of 324 kN [72 kips]. A lower bound force of 36 kN [8 kips] was used instead of zero to ensure continuous contact between the actuator and girder throughout the tests. The upper bound force was selected so the load range (320 kN [72 kips]) would be equal to the specified weight of a standard HS20 truck, and because it imposed maximum interface shear stresses approximately equal to half the nominal strength of Girder #1 (Table 3).

Before any cycles were applied, each specimen was subjected to two cycles of low frequency (0.02 Hz) linearly-varying force, from 36 to 360 kN [8 to 80 kips], to allow for recording of baseline displacement and strain data. The cyclic force was then applied in 20 phases, with each loading phase consisting of 10^5 cycles of force applied as a sinusoidal function with a frequency of 2 Hz. The number of cycles and actuator force were recorded throughout each phase. After each phase was completed, two cycles of low-frequency linearly-varying force were applied following the same protocol as the initial load step for collection of data from all instrumentation.

The calculated increment of interface shear stresses, based on a force increment of 320 kN [72 kips], is shown in Table 3 for each specimen. The interface shear stress was calculated assuming the shear force transferred across the interface on each half of the girder was equal to the compression force in the deck due to midspan moment (with the neutral axis depth calculated assuming uncracked transformed section properties). This interface shear force was then divided by the contact area between the girder and deck, based on a width of 200 mm [8 in.] for Girders #1 and #2 and 910 mm [36 in.] for Girder #3.

Table 3 also shows the nominal strength calculated according to the ACI Building Code (2014) and AASHTO Specification (2012) and the ratios of interface shear stress demand to capacity. The nominal strength calculated according to the AASHTO Specification was based on

Eq. 1. The cyclic loading imposed an increment of interface shear stress in Girders #1, #2, and #3 equal to 42, 19, and 7.7% of the nominal strength according to the AASHTO Specification. The ACI Building Code provisions for horizontal shear strength in composite flexural members differ based on whether the factored shear force V_u exceeds $\Phi(500 b_v d)$. If $V_u \leq \Phi(500 b_v d)$ and $A_v \geq A_{min}$, where Φ is 0.75, nominal horizontal shear strength is calculated with Eq. 2a for intentionally roughened interfaces (Girders #2 and #3) and Eq. 2b otherwise (Girder #1). Where the factored shear force V_u exceeds $\Phi(500 b_v d)$, V_{nh} is calculated with Eq. 3.

$$V_{nh} = min\left[\lambda\left(260 + 0.6\frac{A_v f_{yt}}{b_v s}\right) b_v d, 500 b_v d\right] \qquad \text{Eq. 2a}$$

$$V_n = 80 b_v d \qquad \text{Eq. 2b}$$

$$V_{nh} = \mu_{ACI} A_{vf} f_y \qquad \text{Eq. 3}$$

In Table 3, ACI Building Code (2014) nominal shear strength was calculated with $80 b_v d$ for Girder #1 and $\lambda(260 + 0.6\frac{A_v f_{yt}}{b_v s}) b_v d$ for Girders #2 and #3. The cyclic loading imposed an increment of interface shear stress in Girders #1, #2, and #3 that was 160, 26, and 9.0% of the nominal strength according to the ACI Building Code.

Girder Stiffness

Force was proportional to displacement for all loading cycles. The stiffness of each specimen, calculated as the slope of a linear best-fit line, is given in Table 4 for data collected prior to loading, after 10^6 cycles, and after 2×10^6 cycles. Table 4 also has the estimated specimen stiffness for both fully composite and non-composite action, including both flexural and web shear contributions to deflection. For the fully composite case, stiffness was calculated accounting for the deck not extending to the support. For calculating flexural deformations, uncracked transformed section properties were assumed (I_{tr} of the composite girder was 8,410,000 cm^4 [202,000 $in.^4$]). For calculating web shear deformations, only the area of the web was considered active (150 by 1070 mm [5.9 by 42 in.] for the composite section and 150 by 890 mm [5.9 by 35 in.] for the non-composite section), as recommended by Iyer (2005). The modulus of elasticity of the concrete was calculated to be 35,500 MPa [5,150 ksi] based on Eq. 4 (f_c' was taken as 55 MPa [8 ksi]) and the shear modulus was assumed equal to $0.4E_c$. Approximately one third of the calculated deflection was attributable to web shear deformations.

$$E_c = 33{,}000 K_{1a} {w_c}^{1.5} \sqrt{f_c'} \qquad \text{Eq. 4}$$

The initial stiffness of each specimen was between the stiffnesses calculated for composite and non-composite action, but closer to the value calculated for composite action. The initial stiffnesses of Girders #1 and #2 were similar and slightly less than the initial stiffness of Girder #3. It is likely that the larger contact area between the deck and girder resulted in the slightly greater composite stiffness of Girder #3. More importantly, the changes in specimen stiffness after 10^6 and $2{\times}10^6$ cycles of load showed that the repeated loading caused insignificant changes in stiffness for Girders #2 and #3, whereas Girder #1 ended up with a reduction in stiffness of approximately 6.8% after both 10^6 and $2{\times}10^6$ cycles.

To quantify the effects of the fatigue loading on stiffness, a stiffness ratio was calculated as the stiffness of each girder after each loading phase divided by its initial stiffness. The stiffness ratio is plotted versus the number of loading cycles in Fig. 8 for the three specimens. For Girder #1, a decrease in stiffness ratio of 4.5% is evident after the first phase of loading (10^5 cycles). The stiffness ratio then continued to decrease gradually until it stabilized at approximately 6.8% less than the initial value after 10^6 cycles. Girders #2 and #3 exhibited a reduction of approximately 1% in stiffness ratio within the first 10^5 cycles of loading, and then remained stable throughout the remainder of the test. Results are not reported for Girder #2 after 13×10^5 cycles because of an equipment malfunction that occurred 46,000 cycles into phase 14 of the loading protocol that resulted in a 5-month gap in testing that the other specimens were not subjected to. To provide parity among specimens before loading them to failure, Girder #2 was loaded up to the same 2×10^6 cycles imposed on the other specimens after the equipment was repaired. The long pause, however, allowed for time-dependent effects to skew the test results after the test was resumed.

Interfacial Slip

Relative slip between the ends of the deck and the girder was calculated based on measurements taken after each phase of loading. Relative slip was calculated as the displacement measured with the LVDTs placed at each end of the deck, along the girder centerline (L1 and L2 in Fig. 2). Calculated slip values were corrected for shortening of the top surface of the girder due to flexure between the end of the deck and the position of the LVDT stand. The correction at 360 kN [80 kips] of load was 0.017 mm [0.00065 in.] for all specimens, based on the strain estimated at the top of the girder from first principals. The slip measured by each LVDT at 360 kN [80 kips] of force during the slow loading cycles is plotted versus loading cycle number in Fig. 9(a). As expected, Girder #1 exhibited the largest relative slips (0.033 and 0.046 mm [0.0013 and 0.0018 in.]) and Girder #3 exhibited the smallest relative slips (0.02 and 0.025 mm [0.0008 and 0.0010 in.]). Given that Girder #3 had 4.5 times the roughened area of Girder #2 (910 mm [36 in.] width compared with 200 mm [8 in.] width), it is notable that Girder #2 exhibited only approximately 50% more slip than Girder #3. The slip recorded for these specimens was close to 0.025 mm [0.001 in.], the slip reported by Chung and Chung (1976) to be critical for specimens under cyclic loading.

The ratio of relative slip at a given load cycle to the relative slip measured prior to the fatigue loading is plotted in Fig. 9(b). Although the slip ratio was very sensitive to measurement noise, an increase is indicative of an increase in the flexibility of the girder-deck interface. For Girder #1, the slip ratio for L1 increased to approximately 1.05 after the first 10^5 cycles of loading and then continued to increase gradually to approximately 1.09 after 2×10^6 cycles. For Girder #2, the slip ratio for L2 also increased to approximately 1.06 after the first 10^5 cycles of loading, but it then remained stable. All other measurements of relative slip were stable throughout the tests.

Concrete Surface Strains

Figure 2 shows the strain gauge locations and designations. Figure 10 shows the profile of surface strains measured at midspan, at a force of 360 kN [80 kips], after each of the 20 phases of loading for each specimen. In Fig. 10, the solid and dashed inclined lines represent the strain distribution calculated from first principles for fully composite and non-composite action, respectively. Strains were calculated assuming the girder and deck concrete strengths were 69 and 34 MPa [10 and 5 ksi] and using a transformed section based on concrete moduli calculated using Eq. 4. Strains from shrinkage, creep, and prestressing forces were neglected when calculating the expected strain profiles to allow for direct comparison with strain data, which were measurements of changes in strain due to imposed loads. Gauge S5 did not work for Girders #1 and #2.

Although measured strains varied somewhat among the loading cycles, in all cases the measured strains were closer to the solid line than the dotted line. Strains were generally close to those expected for fully composite action throughout the tests, which indicates that although there were small increases in flexibility of the girder-deck interface (indicated by changes in girder stiffness ratio and deck slip ratio), the interface continued to transfer shear throughout the tests. This is true even near the completion of the test of Girder #1, indicating that despite a 6.8% loss of stiffness the beam was still largely composite near midspan.

In all three specimens, strains recorded with S13, located 25 mm [1 in.] from the top of the deck and 610 mm [24 in.] from the centerline, were much smaller than those recorded with S14, located on the top of the deck 380 mm [15 in.] from the centerline. Strains were therefore not uniform across the deck width. This was true even in Girder #3, which had a 910 mm [36 in.] wide bonded area between the girder and deck. The effective deck width therefore did not appear to be sensitive to the width of the girder-deck interface.

To evaluate the variation of strains with the number of loading cycles, a strain ratio was calculated for each gauge as the ratio of strain at a load of 360 kN [80 kips] measured after the completion of each phase to the strain at a load of 360 kN [80 kips] measured before applying cyclic forces. The strain ratio is plotted versus number of loading cycles in Fig. 11 for selected gauges in Girders #1 and #2. The gauges selected for Fig. 11 were gauges that had significant changes during the test. All other gauges had strain ratios near one and are not plotted (including all gauges for Girder #3). After the first 10^5 cycles applied to Girder #1, strains measured with S4 and S6 increased approximately 40 and 80 percent, respectively, with respect to initial values (Fig. 11(a)). These strain ratios continued to increase until becoming stable at approximately 7×10^5 cycles. The increase in compressive strain in the girder top flange is consistent with a shift away from fully composite behavior. Unlike S4 and S6, the strains measured with S12, S13 and S14 dropped approximately 60, 50, and 20% respectively. Again, these changes are consistent with a shift away from fully composite behavior near midspan. For Girder #2, only data from S3 exhibited a measureable change in strain amplitude (Fig. 11(b)). Strains measured with S3 dropped 30% after the first 10^5 cycles and continued to drop to approximately 50% of the initial value after 5×10^5 cycles. This isolated change in data measured with S3 of Girder #2 was not consistent with other measurements. It is likely the change in S3 strains was due to a through-thickness crack that was noted after completion of 2×10^6 cycles in the deck approximately 3 in. from S3.

Summary

Fatigue loading caused changes in the response of Girders #1, #2, and #3 that were important, minor, and negligible, respectively. This correlates with the calculated interface stress demand (Table 3), which was 160, 26, and 9.0% of the nominal stress calculated with ACI Building Code (2014) provisions and 42, 19, and 7.7% of the nominal stresses calculated with AASHTO Specifications (2012), respectively. The changes noted for Girder #1 were a 6.8% reduction in stiffness, an increase in interface slip along one end of the deck of approximately 8 to 9%, and changes in measured strain consistent with a shift away from fully composite behavior. Regardless, the strain profile and stiffness remained close to those expected for fully composite behavior after 2×10^6 cycles of load. The only notable change observed in Girder #2 was the 7 to 8% increase in interface slip along one end of the deck. Changes in stiffness and measured strains were negligible.

Phase 3: Monotonic Tests

Test Setup, Instrumentation, and Loading Protocol

After 2×10^6 cycles of load to 360 kN [80 kips] were applied to each specimen, and approximately one year after placement of the replacement bridge deck, each of the girders was monotonically loaded at midspan until failure using a test setup similar to that used for the cyclic tests (Fig. 2). There were three changes to the test setup: 1) four 1300-kN [300-kip] capacity hydraulic jacks were used instead of the 490-kN [110-kip] actuator, 2) an array of 77 high-frequency infrared markers were mounted to the specimen (Fig. 2), and 3) the LVDT under the girder (L3 in Fig. 2) was removed. The location of these markers in 3D space was recorded throughout the test. Data from this system were used for calculating deformations of the surface of the specimens throughout the tests.

Load was applied at a consistently slow speed with the four hand-pumped 1300 kN [300 kips] hollow-cylinder hydraulic jacks. While the first 1800 kN [400 kips] of force was applied, loading was paused periodically for specimen observation. Lines were drawn alongside cracks and the applied force was noted. Except for Girder #1, specimens were loaded until failure without pause after reaching 1800 kN [400 kips]. The procedure was altered for Girder #1 to address minor problems in the loading apparatus that are not believed to have altered the results (Li 2017).

Force versus Displacement

Imposed force is plotted versus midspan deflection for each specimen in Fig. 12. Force was taken as the sum of forces imposed by the four hydraulic jacks, measured with independent load cells for each jack, and the weight of the loading frame (22 kN [5 kips]). Midspan deflection was calculated as the average vertical deflection of the markers located along the vertical axis of the girder at midspan minus the average vertical deflection of two markers, each located immediately over one of the supports (see Fig. 2).

The shape of the force-deflection relationship was similar among the specimens. Each began with a linear ascending branch with approximately the same slope. As evident in the Fig. 12 insert, all three specimens had a reduction in stiffness at forces between 890 and 1100 kN [200 and 250 kips] that coincided with or somewhat preceded the first observed inclined web cracks (Table 5). The forces at the transition point indicated in Table 5 correspond to web shear stresses of 2.8, 3.3, and 3.5 MPa [400, 480, and 500 psi] at first cracking, based on a web area of 150 by 1070 mm [5.9 by 42 in.]. The stiffness reduction was significantly less in Girder #3, likely because it had 16 mm [No. 5] transverse bars spaced at 150 mm [6 in.] instead of the 300 mm [12 in.] spacing used in Girders #1 and #2. The difference in transverse reinforcement spacing also caused a difference in the spacing of web-shear cracks, with an average spacing of 150 mm [6 in.] observed for Girders #1 and #2, compared with a spacing of 110 mm [4.5 in.] for Girder #3.

After inclined cracking, force and deflection remained proportional until approximately 1800 kN [400 kips] of force, when flexural cracks were first observed (Fig. 13(a)). After flexural cracks were observed, deflections increased at a much higher rate than force. Deflections greater than approximately 25 mm [1 in.] were associated with negligible changes in force, indicating that the strands were yielding. As shown in Table 5, Girders #1, #2, and #3 reached peak forces of 2420, 2560, and 2690 kN [545, 575, and 605 kips] at deflections of 36, 76, and 64 mm [1.4, 3.0, and 2.5 in.]. It is reasonable that Girder #3 had the greatest strength given that it remained fully composite throughout the tests. Girders #1 and #2 both had slightly less strength than Girder #3 because the deck was only partially composite at later stages of the test. Note that fully composite action until failure need not be the aim in design. In practice stable composite action is only required for the range of expected loads. The three specimens all exhibited good deformation capacity. In terms of maximum deflection, Girder #2 had the largest value of 100 mm [4.0 in.] followed by Girder #3 (64 mm [2.5 in.]) and Girder #1 (48 mm [1.9 in.]).

The modes of failure were somewhat different among the specimens. At large deflections, the deck on Girder #1 exhibited a wide flexural crack under the loading point (Fig. 13(b)) that was not associated with underlying cracks in the girder top flange, indicating that the girder and deck were not fully composite late in the test. At a deflection of 48 mm [1.9 in.], a sudden and explosive web shear failure occurred on the east end of the girder (Fig. 13(c)) that caused inclined cracks to extend through the bottom flange to the pin support and through the top flange of the girder near midspan. Both Girders #2 and #3 were loaded until they exhibited compression zone failures in the deck, at large deflections (Fig. 13(d) for Girder #2). Prior to failure, cracks in the deck near midspan of Girder #2 were not connected to cracks in the girder top flange, and slip between the deck and girder was evident at both ends late in the test. In Girder #3, deck cracks were continuous with underlying cracks in the girder flange, evincing closely composite action. Regardless, the occurrence of compression failures in the decks of Girders #2 and #3 are evidence that both continued to transfer shear across the girder-deck interface until failure.

Interfacial Slip

Relative slip between the girder and deck is plotted in Fig. 14 versus position at selected force levels. Slip was calculated at each of the twelve stations identified in Fig. 2 (1-W through 1-E) based on position data from the 3D position tracking system. Relative slip was calculated as the difference in horizontal position between pairs of markers placed 1 in. above the interface on the deck and 1 in. below the interface on the girder, corrected for girder rotation at that section, which was also calculated from marker data. Positive and negative slip values on the east and west sides, respectively, indicate that the bottom of the deck was compressing less than the top of the girder. Although not reported herein, slip measurements from LVDTs placed at each end of the deck closely matched the relative slip calculated at stations 1-E and 1-W. For Girder #1, data from three stations near midspan are omitted due to a localized malfunction of the data acquisition system.

The plotted data for Girder #1 (Fig. 14(a)) show that slip was small (less than 0.25 mm [0.01 in.]) up to approximately 2000 kN [450 kips]. As the force increased to 2050 kN [460 kips], the slip on the east half increased to between 0.5 and 0.8 mm [0.02 and 0.03 in.], indicating that a crack likely formed along the interface. This is much larger than the critical slip of 0.13 mm [0.005 in.] identified by Hanson (1960) for monotonically loaded girders. Slip increased somewhat proportionally with force until approximately 2200 kN [500 kips], beyond which slip increased while force remained relatively constant due to flexural yielding. At peak strength the slip was as large as 4.3 mm [0.17 in.] at the east end of the deck. Throughout the test, slip was much larger on the east half of the girder than on the west half. On the west half of the girder, slip remained less than approximately 0.25 mm [0.01 in.] throughout the test (except for at the far west end of the deck were slip was 0.64 mm [0.025 in.] at peak force). This lopsided slip indicates that after interface cracking developed on the east half of the girder, the cracked interface had insufficient shearing strength to force cracking to extend to the west half.

For Girder #2, slip was again small (less than 0.25 mm [0.01 in.]) until the force increased to 2140 kN [480 kips], when slip along the west half of the girder increased to between 0.25 and 0.76 mm [0.01 and 0.03 in.] while remaining near zero along the east half of the girder (Fig. 14(b)). This is only slightly larger than the load at which cracking occurred in Girder #1 (2050 kN [460 kips]). Troweled and roughened interfaces therefore developed cracking at similar loads. When the force exceeded 2200 kN [500 kips], slip along the east half of the girder suddenly increased to between 0.13 and 0.51 mm [0.005 and 0.02 in.], indicating that cracking occurred along parts of the east half of the span. This shows that after cracking, the roughened interface on the west half of Girder #2 had sufficient strength to force cracking to develop on the east end, despite having slip values much greater than Hanson's critical slip of 0.13 mm [0.005 in.]. Slip continued to increase along both halves of the girder as load increased, with peak values of 5.1 and 3.6 mm [0.20 and 0.14 in.] on the east and west halves, respectively.

Interface slip was near zero throughout the test of Girder #3, as shown in Fig. 14(c).

Interface Shear Stress

For Girder #1, interface cracking occurred when the imposed force was approximately 2050 kN [460 kips], resulting in an interface shear stress at cracking of 7.6 MPa [1100 psi], significantly greater than the 2.2 MPa [320 psi] of strength expected based on the push-off tests by Li, Lequesne, and Matamoros (2018) or the nominal strengths in Table 3. The same push-off test results also indicated that first cracking and peak stress generally coincide for troweled interfaces, so 7.6 MPa [1100 psi] was likely the peak interface shear stress for Girder #1. Subsequent loads were then carried in a partially composite manner, with some of the compression zone forces shifting to the top flange of the girder. This is consistent with observation, as no cracking of the top flange was observed until the web shear failure occurred.

For Girder #2, interface shear stress at first cracking on the west end of the girder was 7.9 MPa [1140 psi] (the imposed force was 2140 kN [480 kips]). Unlike Girder #1, Girder #2 retained sufficient post-cracking shear strength to force cracking to also develop on the east end. This is consistent with results from many prior push-off tests, which have shown that the peak shear strength of roughened interfaces exceeds the cracking strength (through shear friction).

Unlike the other two specimens, the maximum interface shear stress imposed during the test of Girder #3 (1.65 MPa [240 psi]) was at peak force. This stress was lower than in other specimens due to the large bonded interface area, and thus no interface cracking was observed.

CONCLUSIONS

The following conclusions were drawn based on the reported experimental results:

1. Roofing felt is easy to install over girder flanges, significantly reduces the effort required for bridge deck removal, and dramatically reduces damage to girders caused by hammer impact by eliminating the need for use of chipping hammers over flanges. Troweled surfaces without bond breakers do not achieve these aims, as relatively strong bond develops at the joint.
2. Regardless of connection detail, girders are vulnerable to saw-cut damage. Saw-cut damage could be reduced by a) limiting the number of cuts, b) setting the maximum cut depth to less than the deck thickness near the girder, and either c) identifying the location of interface shear reinforcement before saw-cutting (e.g. with GPR rebar locators), or d) eliminating transverse cuts through the deck over the girder web where interface shear reinforcement is located.
3. Casting and removal of a bridge deck alters the top surface of bridge girders, although it was possible to return the surfaces of all three girders to a condition qualitatively similar to their original state with reasonable effort.
4. Interface area had a small effect on girder stiffness. Girder #3, with a bonded interface area that was 4.5 times that of Girders #1 and #2, was 5% stiffer than Girders #1 and #2. Measured girder stiffness was 5 to 10% less than the stiffness calculated for composite action (considering web shear deformations) and 45 to 55% greater than for non-composite action.

5. Composite action can be developed across partially troweled/partially debonded and partially-roughened/partially debonded interfaces after deck replacement. Specimens with either detail maintained full composite action throughout 2×10^6 cycles of loading to 42 and 19% of the nominal shear strength, respectively, per the 2012 AASHTO LRFD Specification (160 and 26% of nominal strength per the 2014 ACI Building Code). Specimens also remained composite far beyond the nominal interface shear strength when monotonically loaded to failure.
6. Specimens with partially troweled and partially roughened interfaces exhibited interface cracking at similar levels of applied force. After cracking, the roughened interface was better able to control slip and transfer force across the interface than the troweled interface, which exhibited significantly larger slip and no evidence of residual interface shear strength.
7. At peak girder strength, even specimens with large interfacial slip (up to 5 mm [0.20 in.]) maintained partially composite action sustained by dowel action. This is evinced by Girder #2, which exhibited a compression zone failure in the deck after large interfacial slip.
8. Changes in measured response under repeated loading must be interpreted carefully in the field. Although large (>100%) changes in concrete surface strains and small (<10%) changes in both girder stiffness and interface slip under fatigue-type cyclic loading appeared to indicate a shift away from composite action in Girder #1, girder strength, stiffness, and the profile of concrete strains all indicated that composite action was sustained through 2×10^6 cycles of loading.

ACKNOWLEDGEMENTS

Financial support was provided by the Kansas Department of Transportation (Grant No. C2036).

Coreslab Structures donated the precast concrete girders. Input from Shawn Schwensen and Colby Farlow of the Kansas Department of Transportation is gratefully acknowledged. The conclusions are those of the authors and do not necessarily represent the views of the sponsors.

NOTATION

A_{cv} = Area of concrete engaged in shear transfer

A_{min} = Minimum area of shear reinforcement within s (the larger of $0.75\sqrt{f_c'}\frac{b_w s}{f_{yt}}$ and $50\frac{b_w s}{f_{yt}}$)

A_v = Area of shear reinforcement within s

A_{vf} = Area of shear reinforcement crossing perpendicular to the shear plane within A_{cv}

b_v = Contact surface width

b_w = Girder web width

c = Cohesion factor

d = Distance from the extreme compression fiber to the longitudinal reinforcement centroid

E_c = Modulus of elasticity of concrete

f_c' = Specified concrete compressive strength

f_{ci}' = Concrete compressive strength at the time of initial prestress (taken as $0.8f_c'$)

f_y = Reinforcement yield stress

f_{yt} = Transverse reinforcement yield stress

I_{tr} = Transformed moment of inertia

K_1 = Fraction of concrete strength available to resist interface shear

K_{1a} = Correction factor for aggregate source (taken as 1.0)

K_2 = Limiting interface shear stress

P_c = Permanent net compressive force normal to the shear plane

s = Spacing between layers of interface reinforcement, measured parallel to girder axis

V_{nh} = Nominal interface shear strength per ACI Building Code (2014)

V_{ni} = Nominal interface shear strength per AASHTO Specification (2012)

V_u = Factored shear force demand

w_c = Concrete density (taken as 22.8 kN/m^3 [0.145 kcf])

λ = Modification factor for lightweight concrete

μ = Coefficient representing the surface preparation at the interface

Φ = Strength reduction factor

REFERENCES

American Association of State Highway and Transportation Officials (AASHTO). (2012). *AASHTO LRFD Bridge Design Specifications (6th Edition)*, Washington, D.C.

American Association of State Highway and Transportation Officials (AASHTO). (2012). *Standard Specification for Air-Entraining Admixtures for Concrete (M154MM154-12-UL)*, Washington, D.C.

American Concrete Institute (ACI). (2014). "Building Code Requirements for Structural Concrete and Commentary". *ACI 318-14*, Farmington Hills, MI.

Assad, S. A. and Morcous, G. (2015). "Evaluating the Impact of Bridge-Deck Removal on the Performance of Precast/Prestressed Concrete I-Girders". *ASCE Journal of Performance of Constructed Facilities*, 30(3), 11 pp.

ASTM A416/A416M-17a (2017). *Standard Specification for Low-Relaxation, Seven-Wire Steel Strand for Prestressed Concrete*, ASTM International, West Conshohocken, PA.

ASTM A615/A615M-16 (2016). *Standard Specification for Deformed and Plain Carbon-Steel Bars for Concrete Reinforcement*, ASTM International, West Conshohocken, PA.

ASTM C39/C39M-17b (2017) Standard Test Method for Compressive Strength of Cylindrical Concrete Specimens, ASTM International, West Conshohocken, PA.

ASTM C260/C260M-10a (2016). *Standard Specification for Air-Entraining Admixtures for Concrete*, ASTM International, West Conshohocken, PA.

ASTM C494/C494M-15 (2015). *Standard Specification for Chemical Admixtures for Concrete*, ASTM International, West Conshohocken, PA.

ASTM D4869/D4869M-16a (2016). *Standard Specification for Asphalt-Saturated Organic Felt Underlayment Used in Steep Slope Roofing*, ASTM International, West Conshohocken, PA.

Badoux, J. C. and Hulsbos, C. L. (1967). "Horizontal Shear Connection in Composite Concrete Beams under Repeated Loads". *ACI Journal*, 64(12), 811-819.

Beacham, M. and Derrick, D. (1999). "Longer Bridge Spans with Nebraska's NU I-Girders". *TR News*, 202, 42-43.

Chung, H. W. and Chung, T. Y. (1976). "Prestressed Concrete Composite Beams under Repeated Loading". *ACI Journal*, 73(5), 291-295.

Hanson, N. W. (1960). "Precast-Prestressed Concrete Bridges: 2. Horizontal Shear Connections". *Journal of the PCA Research and Development Laboratories*, 2(2), 38-58.

Iyer, H. (2005). *The Effect of Shear Deformation in Rectangular and Wide Flange Sections*. Master's Thesis, Virginia Polytechnic Institute and State University, Blacksburg, VA.

Kahn, L. F. and Slapkus, A. (2004). "Interface Shear in High Strength Composite T-beams". *PCI Journal*, 49(4), 102-110.

Kamel, M. R. (1996). *Innovative Precast Concrete Composite Bridge Systems*. Ph.D. Dissertation, University of Nebraska-Lincoln, Lincoln, NB.

Kansas Department of Transportation (KDOT). (2015). *Standard Specifications for State Road & Bridge Construction*. Kansas Department of Transportation, Topeka, KS.

Li, C. (2017). *Composite Action in Prestressed NU I-Girder Bridge Deck Systems Constructed with Bond Breakers to Facilitate Deck Removal*, Ph.D. Dissertation, University of Kansas, Lawrence, KS, 210 pp.

Li, C., Lequesne, R. D., and Matamoros, A. (2018). *Effects of Partially Debonded Girder-Deck Interface on Interface Shear Strength, Deck Removal, and Composite Action*, *SM Report No. 128*, University of Kansas Center for Research, Lawrence, KS.

Loov, R. E. and Patnaik, A. K. (1994). "Horizontal Shear Strength of Composite Concrete Beams with a Rough Interface". *PCI Journal*, 39(1), 48-69.

Saemann, J. C. and Washa, G. W. (1964). "Horizontal Shear Connections between Precast Beams and Cast-In-Place Slabs". *Journal of the American Concrete Institute*, 61(11), 1383-1410.

Table Captions:

Table 1. Concrete mixture proportions per 0.76 m^3 [1 yd^3] (SSD)

Table 2. Person-hours required for bridge deck demolition

Table 3. Calculated and nominal interface shear stress

Table 4. Girder stiffness

Table 5. Summary of results from monotonic tests

Figure Captions:

Fig. 1. NU900 [NU35] girder specimen reinforcement [1 mm = 0.0394 in.]

Fig. 2. Elevation view of composite girder [1 m = 39.4 in.]

Fig. 3. Girder top flange surface details [1 mm = 0.0394 in.]

Fig. 4. Girder #2 prior to first concrete placement

Fig. 5. Deck removal

Fig. 6. Girder damage after deck removal

Fig. 7. Prior to second deck casting, Girders #3 to #1, left to right

Fig. 8. Ratio of girder stiffness to initial girder stiffness

Fig. 9. Slip at deck ends relative to girder surface [1 mm = 0.0394 in.]

Fig. 10. Strain distribution along girder depth at midspan

Fig. 11. Strain ratio versus number of loading cycles

Fig. 12. Force versus deflection, with insert showing initial response [1 mm = 0.0394 in., 1 kN = 0.225 kip]

Fig. 13. Specimens during and after testing

Fig. 14. Distribution of slip over girder length [1 m = 1000 mm = 39.4 in., 1 kN = 0.225 kip]

Table 1. Concrete mixture proportions per 0.76 m^3 [1 yd^3] (SSD)

Constituent	Girder	Deck
Water (kg [lb])	114 [252]	124 [274]
Cement [a] (kg [lb])	331 [729]	264 [583]
Fine Aggregate [b] (kg [lb])	771 [1700]	853 [1880]
Coarse Aggregate [c] (kg [lb])	517 [1140]	558 [1230]
Air Entraining Admixture [d] (L [oz])	2.1 [70]	0
Water Reducing Admixture [e] (L [oz])	1.0-2.2 [35-75] [f]	0.50 [17]
Measured Density (kg/m^3 [lb/yd^3])	Not reported	2320 [145]

[a] Girder: Type III Portland Cement; Deck: Type I Portland Cement

[b] Girder: KSDOT FA-A compliant aggregate; Deck: Kansas River sand

[c] Girder: MoDot Grade "E"; Deck: limestone (max. size = 19 mm [3/4 in.])

[d] Neutralized vinsol-resin compliant with ASTM C260 and AASHTO M154

[e] Girder: PS 1466; Deck: ADVA 195 (both compliant with ASTM C494)

[f] Exact quantity not reported

Table 2. Person-hours required for bridge deck demolition

Specimen	Saw-cutting	Edges [a]	Middle [b]	Total	Total / Girder #3 Total
Girder #1	4.5	21	9.5	35	75%
Girder #2	4.5	3.0	9.5	17	35%
Girder #3	4.5	33	9.5	47	100%

[a] Portions of deck over girder flange
[b] Portions of deck over girder web

Table 3. Calculated and nominal interface shear stress

Specimen	Shear Stress at Cycle Peak (MPa [psi])	Nominal Strength (MPa [psi])	
		AASHTO	ACI 318-14
Girder #1	0.876 [127]	2.1 [300], 42% [a]	0.55 [80], 160% [a]
Girder #2	0.876 [127]	4.6 [660], 19% [a]	3.4 [490], 26% [a]
Girder #3	0.193 [28]	2.6 [370], 7.7% [a]	2.1 [310], 9.0% [a]

[a] Ratio of shear stress at 320 kN [72 kip] to nominal strength

Table 4. Girder stiffness

Case	Stiffness (MN/m [kip/in.])		
	Girder #1	Girder #2	Girder #3
Prior to Loading	389 [2220]	380 [2170]	408 [2330]
After 1×10^6 Cycles	363 [2070]	377 [2150]	403 [2300]
After 2×10^6 Cycles	363 [2070]	N/A	403 [2300]
Calculated Stiffness (composite)			426 [2430]
Calculated Stiffness (non-composite)			263 [1500]

Table 5. Summary of results from monotonic tests

Case	Girder #1	Girder #2	Girder #3
Force at Transition Point (kN [kip])	890 [200]	1070 [240]	1110 [250]
Force at First Observed Crack (kN [kip])	890 [200]	1110 [250]	1330 [300]
Maximum Force (kN [kip])	2420 [545]	2560 [575]	2690 [605]
Deflection at Maximum Force (mm [in.])	36 [1.4]	76 [3.0]	64 [2.5]

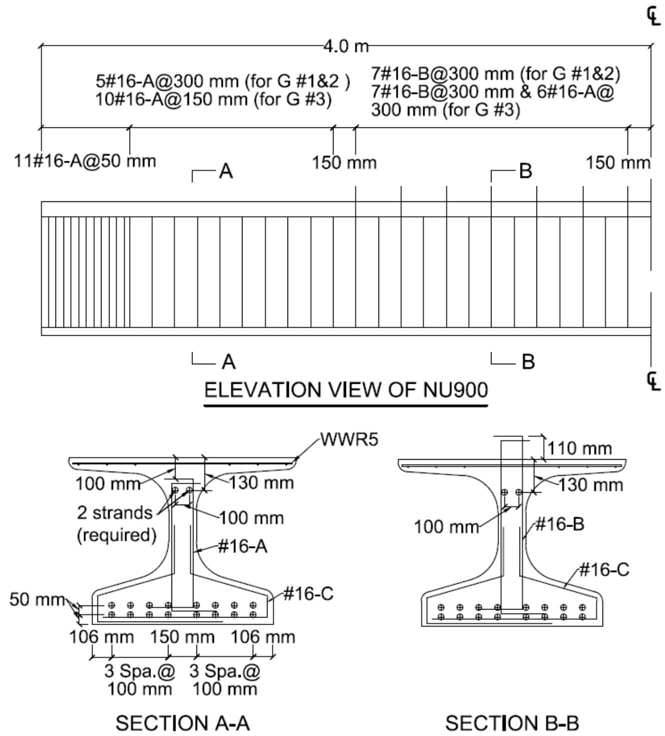

Fig. 1. NU900 [NU35] girder specimen reinforcement [1 mm = 0.0394 in.]

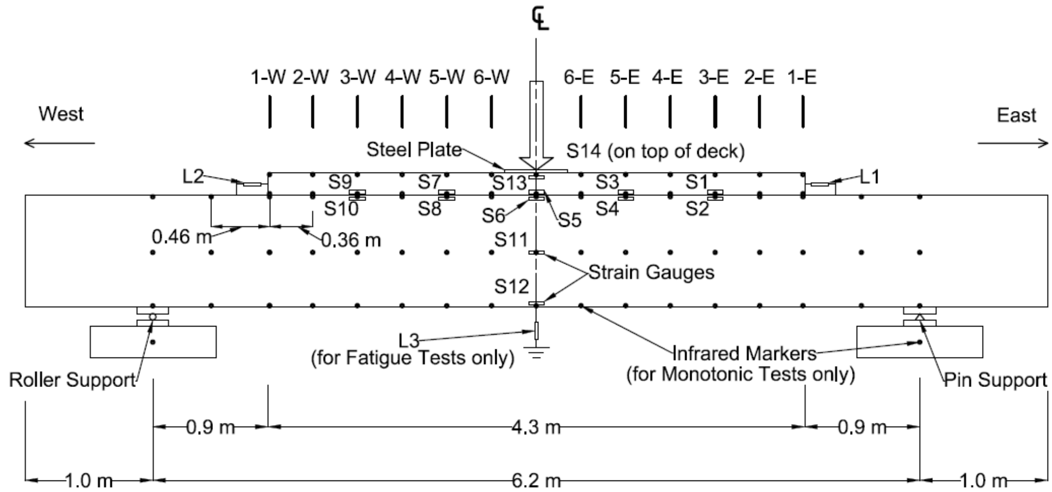

Fig. 2. Elevation view of composite girder [1 m = 39.4 in.]

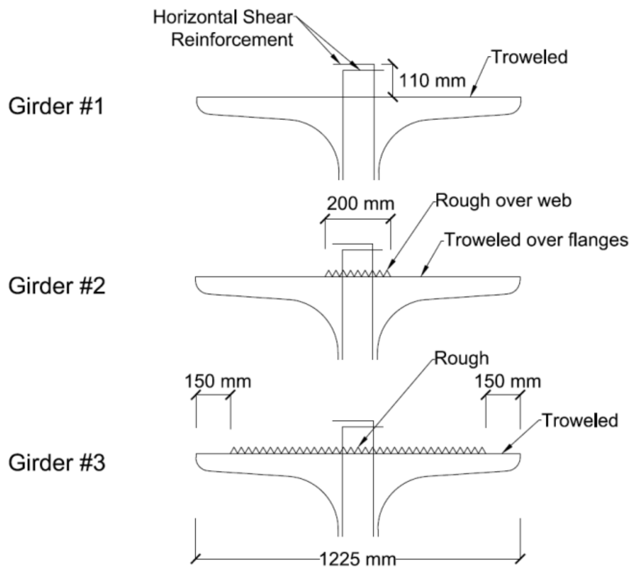

Fig. **3**. Girder top flange surface details [1 mm = 0.0394 in.]

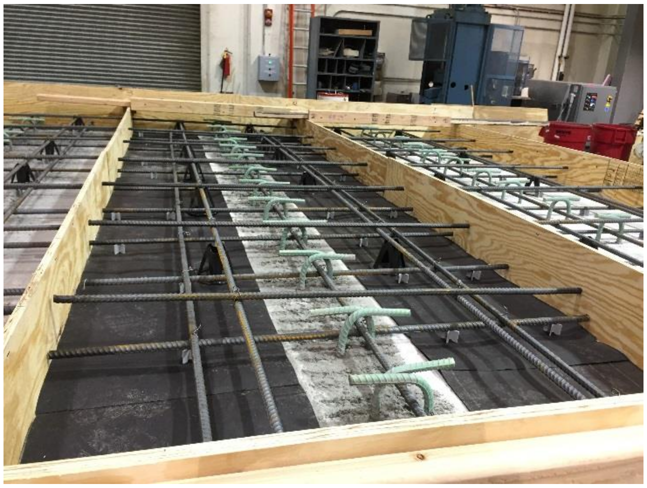

Fig. 4. Girder #2 prior to first concrete placement

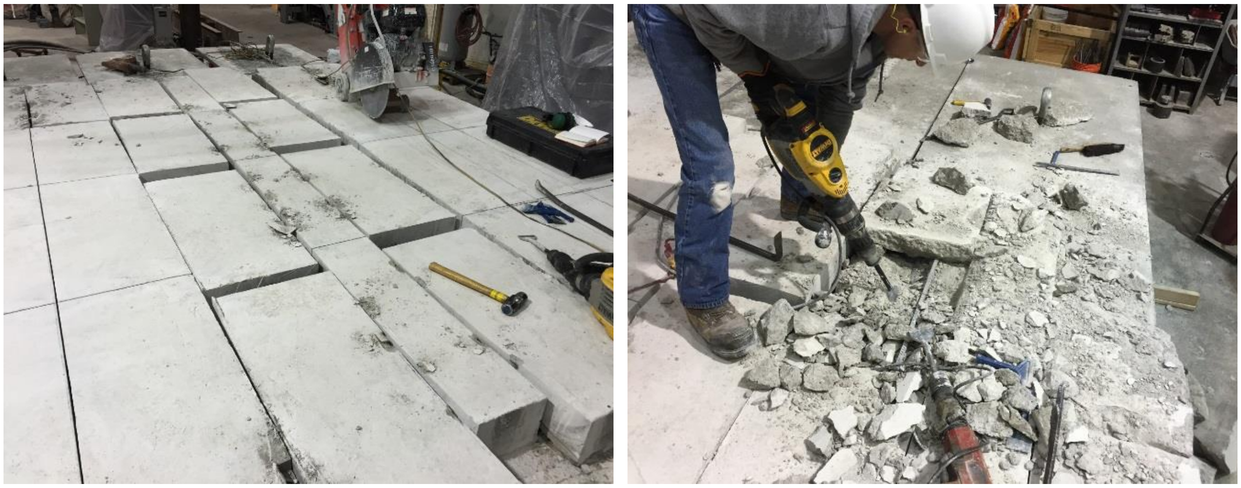

(a) Saw-cut decks and edge pieces over roofing felt (Girder #2)

(b) Edge sections on troweled flange (Girder #1)

Fig. 5. Deck removal

(a) Girder #1: Crater in girder top flange (b) Girder #3: Broken flange tip

Fig. 6. Girder damage after deck removal

Fig. 7. Prior to second deck casting, Girders #3 to #1, left to right

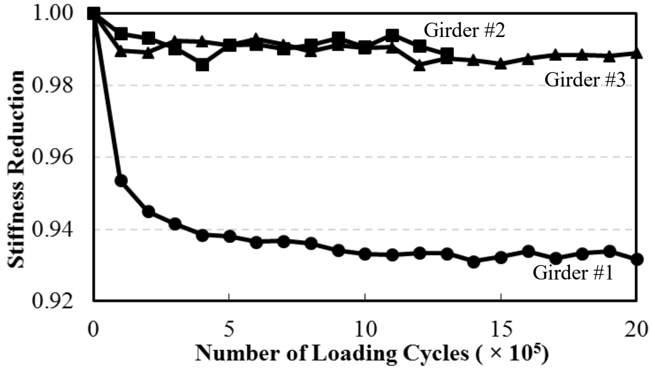

Fig. 8. Ratio of girder stiffness to initial girder stiffness

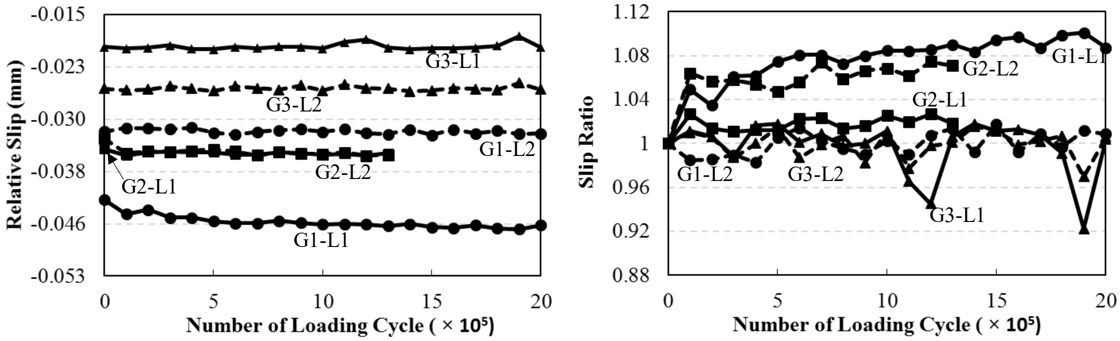

(a) Relative Slip at 320 kN [72 kips]   (b) Slip Ratio

Fig. 9. Slip at deck ends relative to girder surface [1 mm = 0.0394 in.]

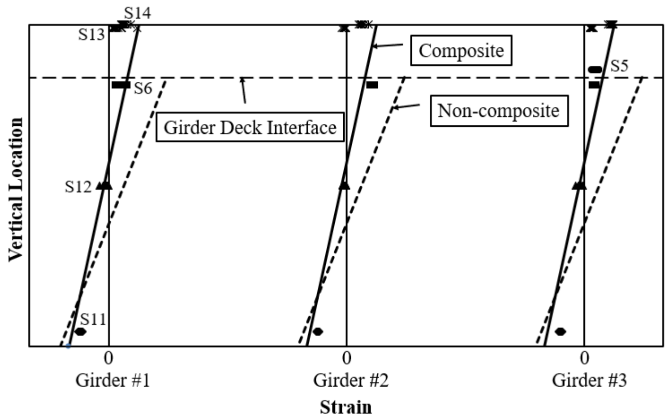

Fig. 10. Strain distribution along girder depth at midspan

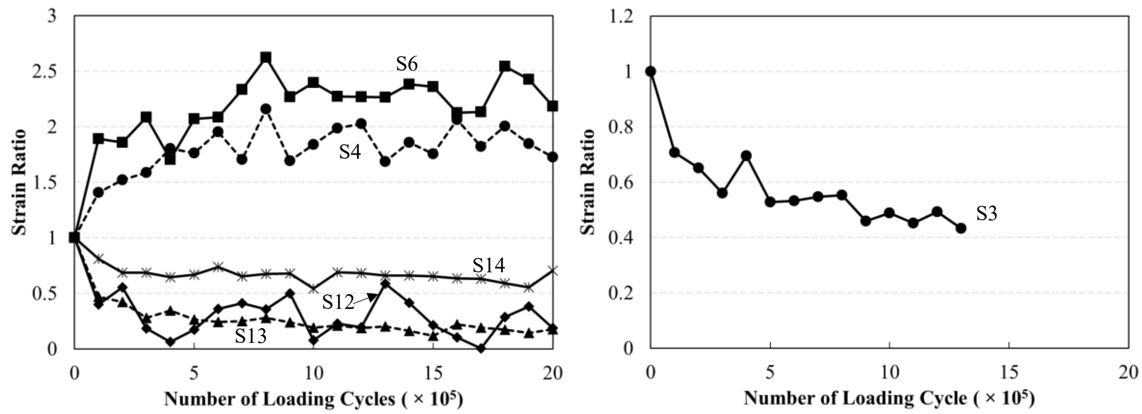

(a) Girder #1 (b) Girder #2

Fig. 11. Strain ratio versus number of loading cycles

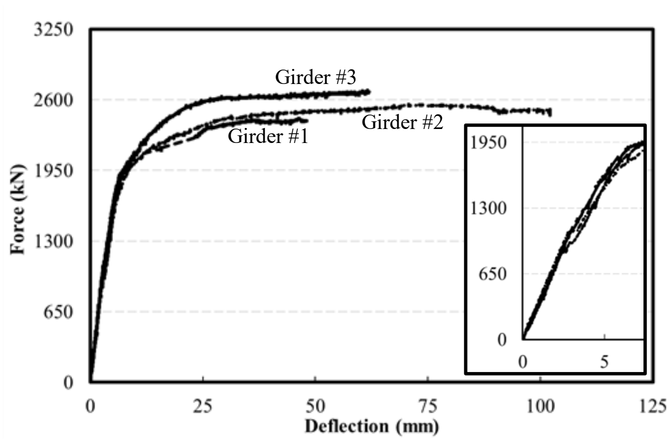

Fig. 12. Force versus deflection, with insert showing initial response [1 mm = 0.0394 in., 1 kN = 0.225 kip]

(a) Cracking at 1780 kN [400 kips] (Girder #2)

(b) Girder #1 near peak load

(c) Girder #1 after failure

(d) Compression zone failure (Girder #2, but also similar to the failure of Girder #3)

Fig. 13. Specimens during and after testing

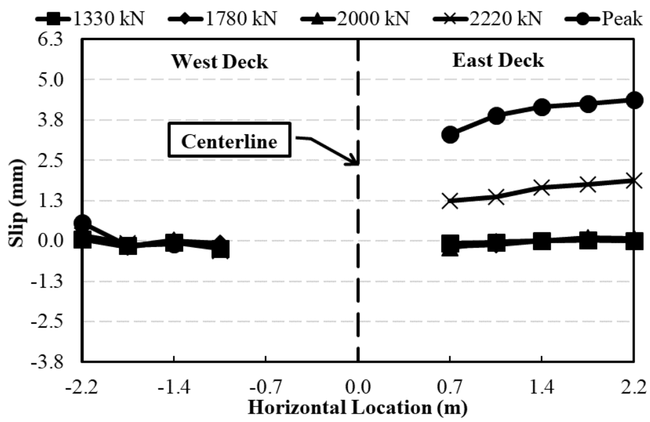

(a) Girder #1

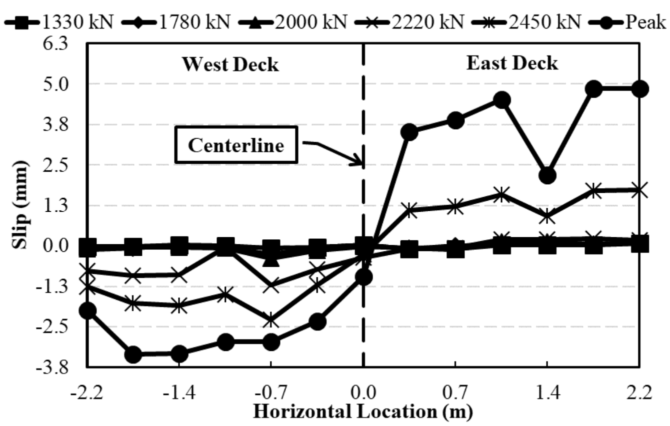

(b) Girder #2

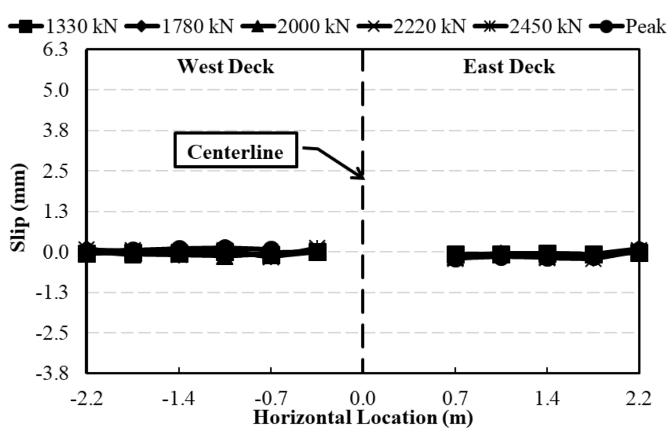

(c) Girder #3

Fig. 14. Distribution of slip over girder length [1 m = 1000 mm = 39.4 in., 1 kN = 0.225 kip]